



HAL
open science

Radiation effects on space-based stellar photometry: theoretical models and empirical results for CoRoT Space Telescope

L. Pinheiro da Silva, G. Rolland, Vincent Lapeyrere, Michel Auvergne

► **To cite this version:**

L. Pinheiro da Silva, G. Rolland, Vincent Lapeyrere, Michel Auvergne. Radiation effects on space-based stellar photometry: theoretical models and empirical results for CoRoT Space Telescope. Monthly Notices of the Royal Astronomical Society, 2008, 384, pp.1337-1343. 10.1111/j.1365-2966.2007.12800.x . hal-03732205

HAL Id: hal-03732205

<https://hal.science/hal-03732205>

Submitted on 16 Oct 2022

HAL is a multi-disciplinary open access archive for the deposit and dissemination of scientific research documents, whether they are published or not. The documents may come from teaching and research institutions in France or abroad, or from public or private research centers.

L'archive ouverte pluridisciplinaire **HAL**, est destinée au dépôt et à la diffusion de documents scientifiques de niveau recherche, publiés ou non, émanant des établissements d'enseignement et de recherche français ou étrangers, des laboratoires publics ou privés.

Radiation effects on space-based stellar photometry: theoretical models and empirical results for *CoRoT* Space Telescope

L. Pinheiro da Silva,^{1,3★†} G. Rolland,^{2†} V. Lapeyrere¹ and M. Auvergne¹

¹Observatoire de Paris-Meudon (LESIA/CNRS), 5 place Jules Janssen, 92195 Meudon, France

²Centre National d'Etudes Spatiales (CNES), 18 av. Edouard Belin, 31401 Toulouse, France

³Centre d'Etude Spatiale des Rayonnements (CESR/CNRS), 7 av. du colonel Roche, 31028 Toulouse, France

Accepted 2007 December 4. Received 2007 December 3; in original form 2007 July 4

ABSTRACT

Convection, Rotation and planetary Transits (CoRoT) is a space mission dedicated to stellar seismology and the search for extrasolar planets. Both scientific programs are based on very high precision photometry and require long, uninterrupted observations. The instrument is based on an afocal telescope and a wide-field camera, consisting of four E2V-4280 CCD devices. This set is mounted on a recurrent platform for insertion in low Earth orbit. The *CoRoT* satellite has been recently launched for a nominal mission duration of three years.

In this work, we discuss the impact of space radiation on *CoRoT* CCDs, in sight of the in-flight characterization results obtained during the satellite's commissioning phase, as well as the very first observational data. We start by describing the population of trapped particles at the satellite altitude, and by presenting a theoretical prediction for the incoming radiation fluxes seen by the CCDs behind shielding. Empirical results regarding particle impact rates and their geographical distribution are then presented and discussed. The effect of particle impacts is also statistically characterized, with respect to the ionizing energy imparted to the CCDs and the size of impact trails. Based on these results, we discuss the effects of space radiation on precise and time-resolved stellar photometry from space. Finally, we present preliminary results concerning permanent radiation damage on *CoRoT* CCDs, as extrapolated from the data available at the beginning of the satellite's lifetime.

Key words: instrumentation: detectors – methods: data analysis – space vehicles: instruments – techniques: photometric.

1 INTRODUCTION

Convection, Rotation and planetary Transits (CoRoT) is a high-precision photometry experience dedicated to stellar seismology and the search for extrasolar planets (Boisnard & Auvergne 2004). The mission is led by the French Space Agency [Centre National d'Etudes Spatiales (CNES)] in association with several French laboratories and international partners in Austria, Belgium, Germany, Spain and Brazil. Both scientific programs require great instrumental stability and long uninterrupted observation runs, which take place simultaneously on adjacent regions of the sky.

The instrument is based on an afocal telescope and a wide-field camera, mounted on a recurrent satellite platform. The focal plane is composed of four 4280-series CCD devices provided by E2V technologies following *CoRoT* specifications. Those are frame transfer, thinned, back-illuminated detectors, and are operated at nearly

–40°C. The image area is composed of 2048 × 2048 pixel, and each pixel is 13.5 × 13.5 μm in size.

The *CoRoT* satellite, recently inserted in polar orbit at 896 km of altitude, is exposed to a radiative environment to which several instrumental components are sensitive. Effects can be expected on the CCDs, the optics and the electronics. The latter is somewhat minimized with the use of radiation hardened components. The effects of the interaction between energetic particles and the lenses are almost limited to fluorescence, and lead to a small increase of the background level.

In this work, we discuss the radiation fluxes perceived by *CoRoT* CCDs and characterize the effects of particle impacts on these detectors. These effects are usually divided in two classes: transient events and permanent damage. The first corresponds to the creation of electron-hole pairs in the CCD, leading to transient artefacts on the acquired images. Permanent damage includes the displacement of silicon atoms, as well as cumulative ionization dose effects which are less significant in modern CCDs.

We start by describing the radiative environment to which the *CoRoT* satellite is exposed. We then present a brief theoretical

*E-mail: leonardo.pinheiro@obspm.fr

†These authors equally contributed to this paper.

description of the most relevant physical phenomena taking place and the radiation flux levels that can be expected with basis on some simplified hypothesis, for better readability and appreciation of the empirical data. In Section 3, the results obtained during the satellite's commissioning phase are presented, with respect to the radiation fluxes reaching the CCD detectors, as well as the statistical characterization of the particle impact trails seen on *CoRoT* images. Finally, we present in Section 4 some preliminary results concerning permanent damage on *CoRoT* CCDs, such as the generation of bright pixels and their evolution in time, which were derived from the first few months of observation.

2 THEORETICAL MODELS

2.1 The near-Earth orbital environment

The radiative environment in low Earth orbit (LEO) is primarily associated with the population of charged particles (protons and electrons) which compose the Earth's radiation belts. The inner radiation belt, particularly, is thought to originate mainly from the by-products of cosmic ray collisions with the upper atmosphere (namely through the beta decay of released neutrons), which can then become trapped around Earth's magnetic field lines. The amount of trapped protons will also depend on the solar activity, due to the expansion of the upper atmosphere and an increased loss of particles in this region.

The theoretical particle fluxes experienced by the satellite, at a given altitude or for a given orbit, can be obtained thanks to environment codes like OMERE, SPACERAD or SPENVIS. In the case of *CoRoT*, the SPACERAD code (see Letaw 1997) has been used for mission analysis before the launch, along with the AE8max and AP8min models for the radiation belts, and DGRF70 for the magnetic field. AE8max and AP8min models correspond to a worst-case scenario for *CoRoT* which is independent of the launch date.

At the low-orbital altitudes in question, the South Atlantic Anomaly (SAA) is the region where the satellite is exposed to the highest doses of radiation, for several minutes. The SAA comprehends the region where the inner radiation belt is closest to the surface of the Earth. It results from the fact that the centre of Earth's magnetic field is offset by 450 km from the geographic centre, while its axis is 11:5 tilted with respect to the planet's axis of rotation.

2.2 *CoRoT*'s protective shielding

CCDs are obviously very sensitive to the kind of ionizing radiation encountered in the LEO environment. Fortunately, the particle fluxes to which detectors are exposed can be significantly reduced with the use of some protective shielding. In the case of *CoRoT*, the focal plane is shielded with 10 mm of aluminum, and some instrument parts themselves represent additional protection against particle impacts in some particular directions.

The radiation flux seen by the CCD detectors is therefore a function of the effective shielding and the local environment spectrum $S_e(\mathbf{P}, E)$, where E is the energy of the incident charged particle. \mathbf{P} is a vector representing the satellite instantaneous position (longitude, latitude, altitude).

From the mathematical point of view, the transmitted spectrum $S_t(\mathbf{P}, E)$ (behind the shield) can be deduced from $S_e(\mathbf{P}, E)$ by means of a transfer function $F(E)$, which depends only on the shielding properties around the CCD (designed shielding plus the satellite itself), and on the particle type. The integral radiation flux $\Phi(\mathbf{P})$ is

then given by a simple numerical integration:

$$\Phi(\mathbf{P}) = \int_0^{\infty} F(E) S_e(\mathbf{P}, E) dE. \quad (1)$$

The transfer function $F(E)$ can be evaluated by numerical simulation by means of a Monte Carlo transport code, such as NOVICE (Jordan 2000). The prior construction of a geometrical and physical model of the shield is nevertheless required.

In the next section, we present an estimation of the radiation fluxes seen by *CoRoT* CCDs, for each class of particle, based on a simplified structure consisting of a solid aluminum sphere with 10-mm radius. Since these 10 mm corresponds to the minimal aluminum equivalent shield thickness around the CCD detectors, the presented figures are worst-case fluxes.

2.3 Estimated radiation fluxes

The computation of transfer functions $F(E)$ based on a simplified shielding model leads to the following lower energy bounds for particles reaching the focal plane: 50 MeV for protons, 4 MeV for electrons going through the shielding and 1 MeV for electrons leading to significant secondary radiation (braking photons which then reach the detector).

Figs 1–3 give a qualitative mapping of the distribution of particle populations above these energy levels. We verify that proton fluxes can be expected almost exclusively at the SAA region, while electrons of energy greater than 4 MeV occur at the south and north auroral zones, at the extremity of the outer radiation belt. Braking photons are generated in both regions, around the poles but also in the SAA, due to the (total or partial) braking of SAA and auroral electrons in the shielding material.

A quantitative analysis of the maximum radiation flux expected behind the shield (i.e. peak values in the case of a full-sphere model) is: 6000 protons $\text{cm}^{-2} \text{s}^{-1}$, 40 electrons $\text{cm}^{-2} \text{s}^{-1}$ and 27 000 photons $\text{cm}^{-2} \text{s}^{-1}$. We verify that protons and braking photons represent the dominant type of radiation at the CCD level.

For electrons and protons, it can be assumed that a charge packet is generated for every single particle going through an active region of the CCD. For braking photons, however, the probabilities of interaction with the detector (the cross-section) are very weak, and most of the photons leave the material before any interaction. These probabilities, for a given photon energy, can be deduced from the well-known absorption coefficients for Silicon (e.g. Wrobel 2005),

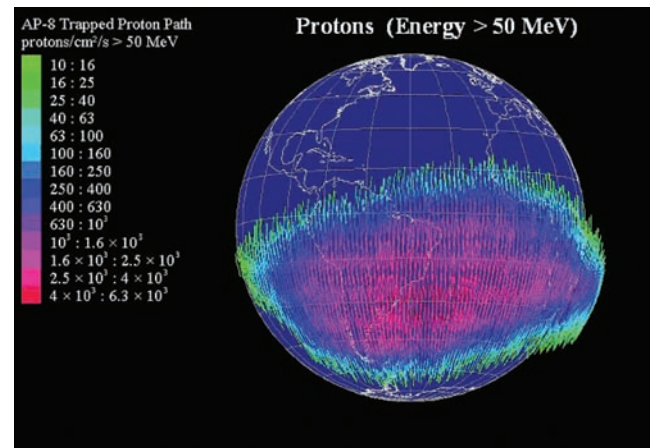


Figure 1. Mapping of the integral flux of protons of energy greater than 50 MeV (outside the satellite) according to the AP8min belt model.

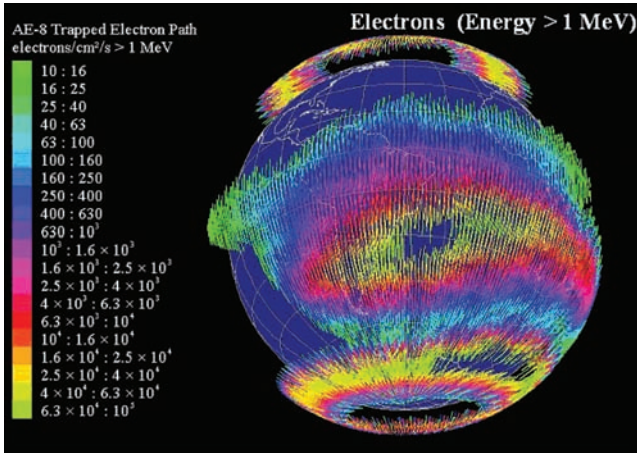


Figure 2. Mapping of the integral flux of electrons of energy greater than 1 MeV (outside the satellite) according to the AE8max belt model. (The holes at the centre of the SAA and in the south auroral zone are artefacts).

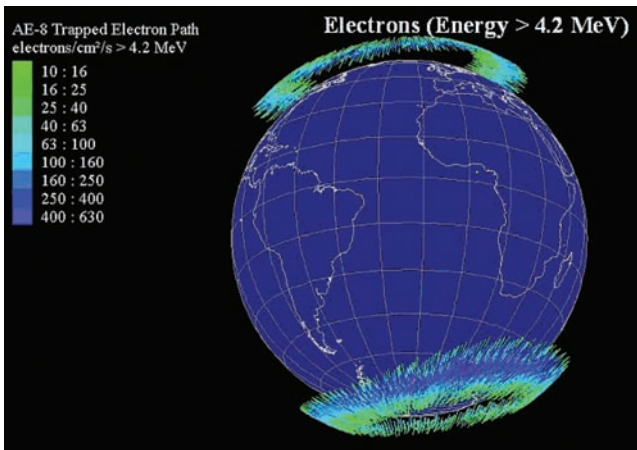


Figure 3. Mapping of the integral flux of electrons of energy greater than 4.2 MeV (outside the satellite) according to the AE8max belt model.

and it turns out that the frequency of occurrence of such an event is far less significant than that of protons impact during SAA crossings, by at least two orders of magnitude.

We conclude that SAA protons are the dominant contribution to the effective radiation flux seen by *CoRoT* CCDs. The next section provides empirical measurements of this radiation and a characterization of its effects on the acquired *CoRoT* data.

3 EMPIRICAL RESULTS

3.1 Measured radiation fluxes

The incoming radiation flux (in $\text{p}^+ \text{cm}^{-2} \text{s}^{-1}$), as a function of latitude and longitude, was empirically characterized in-flight before the opening of the protective shutter placed at the entrance of the *CoRoT* telescope. The objective was to measure the flux seen by the CCD detectors behind the effective shielding (including instrumental components), in complement to the theoretical models presented in the previous sections. The results are supposed to provide a reference during the whole mission duration.

With this purpose, a portion of a CCD image (100×100 pixel) was periodically acquired, at 1 Hz, over 24 h. A global estimation

of the incoming radiation flux was possible thanks to the satellite's polar orbit. To reduce data volume, images acquired outside an enlarged version of the predicted SAA were accumulated on-board, over 128 exposures. Some images obtained inside the SAA are shown in Fig. 4.

The identification of particle impacts in an image requires an iterative approach, since there is a compromise between the detection of all disturbed pixels and the rejection of statistical outliers associated with readout noise. An effective and not overcomplicated approach is the use of a double-clipping technique. Impacted regions are first identified through the application of a high threshold (e.g. 6σ). A lower threshold is then applied (e.g. 3σ), and those pixels contiguous to the first identification are also flagged as impacted. Recurrently, outlying pixels are finally considered as hot (dark current defects), and ignored. That allows for the identification of all impacted pixels without any false detections.

For proper thresholding, a robust estimator of the standard deviation is required, since particle impacts may be very energetic and greatly disturb a classic sigma evaluation. In this work, an estimator based on the median absolute deviation (MAD) was employed (see Olive 2005).

The instantaneous radiation flux corresponding to a single image can be estimated as

$$\bar{\phi}_t = N_{\text{impacts}} / (S_{\text{image}} S_{\text{pixel}}) / (T_{\text{sojourn}} N_{\text{acc}}), \quad (2)$$

where N_{impacts} is the number of unique impacts identified, S_{image} is the image size (in pixels) and S_{pixel} is the surface of a CCD pixel (in cm^2). T_{sojourn} represents the amount of time that the image has been exposed to radiation (i.e. integration time + transfer time + readout time). All those figures can be precisely derived from the CCD readout mode and the timing of each CCD readout operation (1.323 s in this case, for the 100×100 subimage extracted from roughly the centre of a CCD). N_{acc} is the number of image accumulations performed on-board.

The evolution of the instantaneous radiation flux, as well as corresponding satellite orbital data converted into geographic coordinates, is shown in Fig. 5. These three time-series can be put together leading to the radiation flux map shown in Fig. 6. This image illustrates the frontiers of the SAA seen by *CoRoT* detectors behind shielding. The satellite position at the moment of each image acquisition is indicated by a yellow dot.

We verify 8–10 SAA passages per day above a flux threshold of $200 \text{ p}^+ \text{cm}^{-2} \text{s}^{-1}$. Most orbits crossing this region expose the satellite to radiation fluxes exceeding $2500 \text{ p}^+ \text{cm}^{-2} \text{s}^{-1}$ and reaching the peak of $3300 \text{ p}^+ \text{cm}^{-2} \text{s}^{-1}$ in the worst-detected case. The on-board software allows for the activation of specific correction algorithms in this region, at least on bright star targets of the asteroseismology program acquired at 1 Hz. At the same time, measurements on faint stars of the planet finding program are not exploitable due to its longer exposure time (32 s).

These results roughly agree with the predictions presented in Section 2. We verify that modelled and measured radiation fluxes diverge by a factor of 2, which is a reasonable margin given that all theoretical predictions were performed with basis on a worst-case scenario. Most of the model uncertainty is due to the significant amount of material protecting the CCDs (instrumental parts) that has been disregarded during shield calculations. We recall that just the amount of shielding imposed by design (10 mm of Aluminum) had been considered.

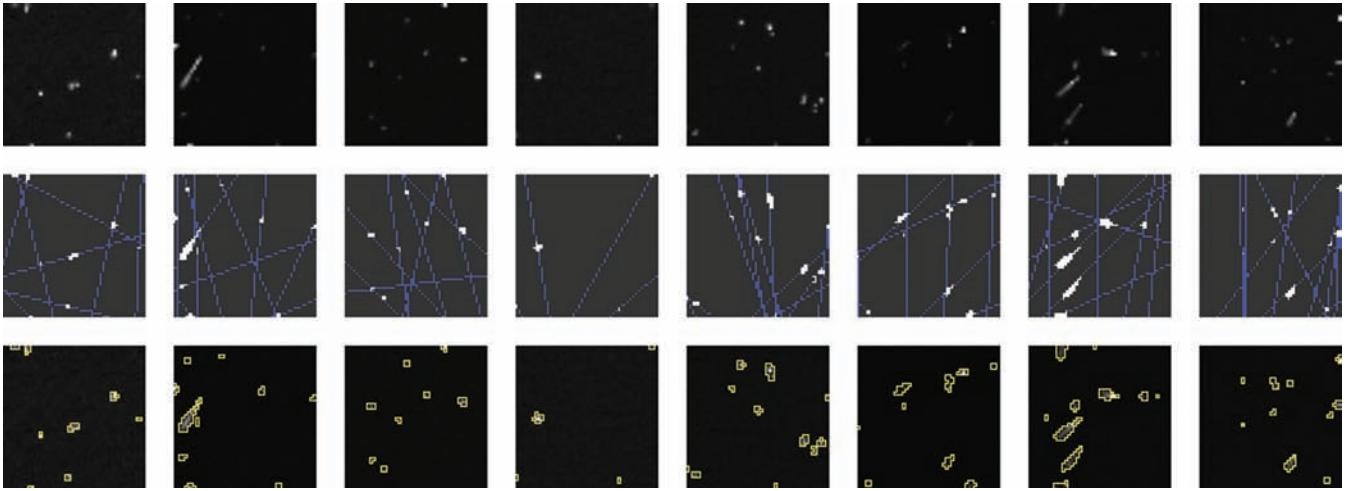


Figure 4. Irradiated CCD images acquired inside the SAA with *CoRoT*. A set of raw images are shown in the top row, along with thresholded images for identification of disturbed pixels (middle row). Blue lines represent a projection of the particle trajectory estimated with local Hough transform. Image segmentation corresponding to the identification of unique particle impacts is shown in the bottom row.

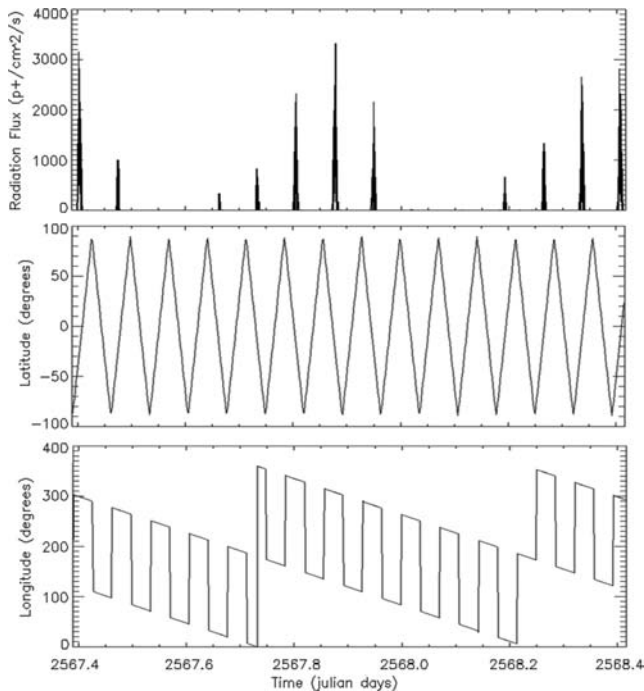


Figure 5. Instantaneous radiation flux (top panel) and corresponding satellite orbital position (latitude and longitude; middle panel and bottom panel, respectively).

3.2 Impacts' characteristics

Particle impacts were characterized, in terms of statistical distributions, after further analysis of the input images (offset and background correction, gain conversion, correction for any instrumental artefacts). The analysed features were the imparted energy per impact (in e^-), the size of an impact trail (in number of disturbed pixels), along with the energy distribution of the brightest pixel of an impact, which is useful for impact detectability purposes. Those results are shown in Fig. 7.

The length of an impact trail on a CCD image derives from pure geometry as a function of the sensitive depth of a CCD pixel (about

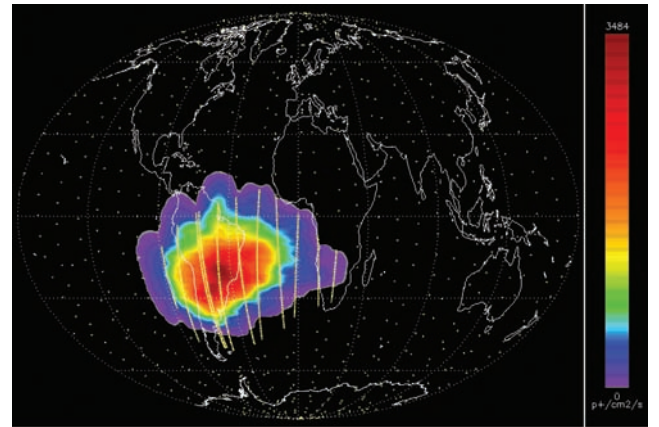


Figure 6. Radiation flux map ($p^+ \text{ cm}^{-2} \text{ s}^{-1}$) derived from a set of periodically acquired images. The satellite position at the moment of each image acquisition is indicated by a yellow dot.

$15 \mu\text{m}$). Indeed, for a pitch angle α , the trail length in μm is given by $\tan \alpha = \text{depth}/\text{length}$. On the other hand, the trail width is not unitary, due to the possibility of diffusion of generated charges to neighbouring pixels before collection at a potential well. The total number of disturbed pixels is a consequence of both variables. Trails spanning over a great number of pixels (corresponding to the tail of the histogram) require very shallow pitch angles ($<1^\circ$), and are therefore very unlikely. On average, 7.9 pixels are disturbed per particle impact.

The imparted energy per impact, also shown in Fig. 7, should not be confused with the energy spectrum of the incident particles, since most leave the CCD before having lost all their kinetic energy. Moreover, the energy imparted by a charged particle to silicon, through ionization, is not directly proportional to the original energy of the particle. However, for the analysis of radiation effects on photometry, the total imparted energy is the relevant quantity. The average energy per impact is about $5160 e^-$. The most violent event registered in 24 h (not shown in that clipped histogram) corresponded to the generation of more than 1.1 Me^- . Considering that

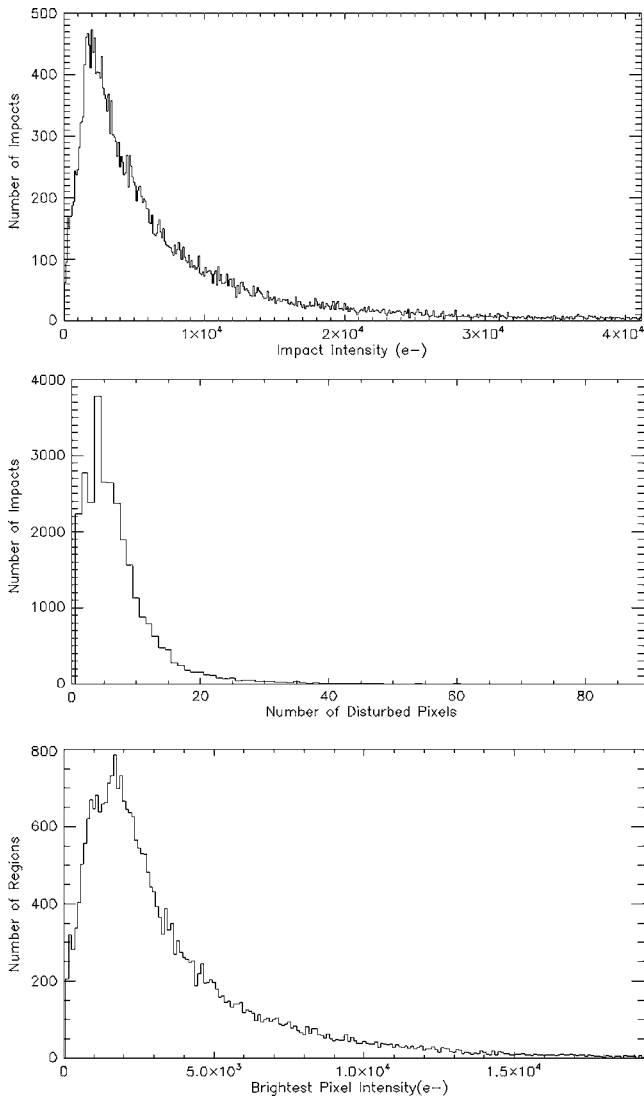


Figure 7. Characteristics of particle impacts in terms of statistical distributions. From top to bottom panel: imparted energy per impact, number of disturbed pixels per impact and intensity of the most disturbed pixel.

3.6 eV is the mean energy required to set an electron free from a silicon atom that corresponded to almost 4 MeV.

3.3 Effect on stellar photometry

The probability of having an impact disturbing a given photometric measurement depends on the instantaneous radiation flux, the image integration time and the size of the projected star image [i.e. the point spread function (PSF)]. This probability is given by the Poisson law. On the other hand, we have, in the most favourable case, around 10^7 collected photons per star image, which corresponds the collected flux for the brightest asteroseismology targets observed by *CoRoT*, given the instrument's collection surface and transmissions.

The scientific objectives require collected photons to be counted with an accuracy on the order of shot noise. Based on the intensity statistical distribution presented in the previous section (and also the small energy spreading, in pixels), we verify that about 90 per cent of the incoming impacts are energetic enough to inval-

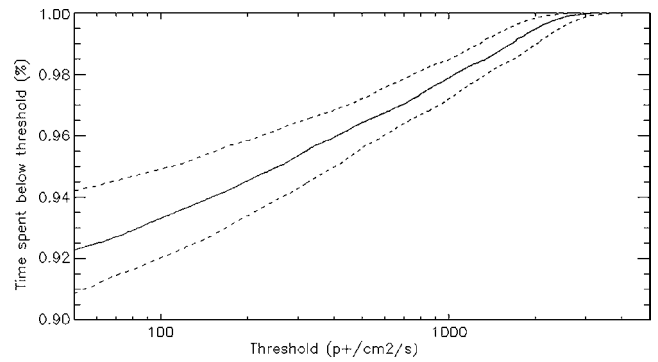


Figure 8. Amount of time spent by the satellite below a radiation flux threshold.

idate an aperture photometry measurement whatever is the stellar magnitude observed by *CoRoT*.

Considering a PSF (and consequently the photometric mask) of a few hundreds of pixels and a 1-s image integration, as in the case of the asteroseismology field, we conclude that under a flux of $200 \text{ p}^+ \text{ cm}^{-2} \text{ s}^{-1}$, chances are better that 50 per cent that an acquired image is subjected to a particle impact. On the planet finding side, PSFs are smaller but the integration time is 32 times higher, lowering the acceptable flux to about $50 \text{ p}^+ \text{ cm}^{-2} \text{ s}^{-1}$.

We present in Fig. 8 the percentage of time spent by the satellite below a given radiation flux threshold. As shown in the figure, the tolerable flux on the seismology side is exceeded during 6 per cent of the total lifetime, leading to a corresponding amount of irradiated images. On aperture photometry data, it has been empirically found that 7 per cent of the measurements are actually flagged as outliers, primarily due to radiation, representing a very significant contribution to the global duty cycle.

4 PERMANENT DAMAGE

Permanent radiation damage in CCD detectors can be divided in two main classes: atomic displacements and total ionizing dose. CCDs operated in inverted mode (Advanced Inverted Mode Operation), as in the case of *CoRoT*, are robust to the ionizing dose effect (which takes place at the silicon-silicon dioxide interface), and displacement damage is therefore the major concern.

Atomic displacement stands for the creation of a defect in the silicon lattice due to the impact of charged particles (usually protons). If the resulting interstitial silicon atom and the corresponding vacancy do not recombine, the resulting defect leads to mid-band energy levels, which greatly facilitates dark current generation by thermal fluctuations.

Depending on the characteristics and position of the defect (for instance in a region of high-electric field), dark rates can be very large, though very localized. The effect is also very dependent on the intermediate energy levels created – energy levels close to mid-gap are the most effective, and dark current generation rates decrease exponentially otherwise (Srouf, Marshall & Marshall 2003). Pixels presenting abnormal dark current rates are denominated bright (or hot) pixels.

Bright pixels usually require specialized procedures in astronomical imaging, for their identification and correction. In time-resolved photometry, those pixels contribute to the total noise and can introduce discontinuities in light curves at the moment of their creation.

Fig. 9 illustrates the creation of two bright pixels due to radiation, as seen in the evolution of the sky background estimated on *CoRoT*

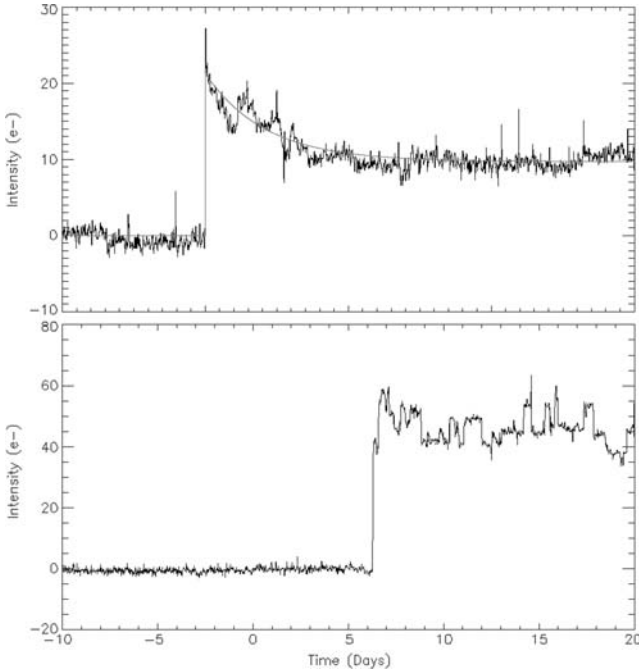


Figure 9. Two examples of light curves illustrating the generation of a bright pixel after a particle impact, seen in the evolution of sky background. The red line is an exponential fit of the bright pixel decrease.

CCD images. That estimation is evaluated as the average over a 10×10 CCD subimage corresponding to an uncrowded region of the sky. Orbital modulations of the components have been rejected by decorrelation with respect to other background estimation points. Each measurement represents an averaging performed on-board over 16 consecutive exposures of 32-s integration time. A median filter, of 10 points width, is applied to reduce the noise on the curves.

In those sky background estimation curves, we notice significant discontinuities of about 20 and 50 electrons, corresponding therefore to bright pixels as intense as 2000 and 5000 e^- /exposure. The step, on each curve, occurs soon after a particle impact during the SAA crossing.

A second aspect seen in these curves, which is even more disturbing for time-resolved photometry, is the fact that the intensity of a bright pixel is not stable but evolves in time. That is due to the mobility of silicon defects, and the possibility of their rearrangement in more stable configurations such as defect clusters or defect impurity complexes. The two curves show different time evolutions, illustrating the different behaviours of bright pixels observed.

The first curve shows a typical evolution – just after its creation, the bright pixel decreases rapidly. This decrease slows down over several days and the bright pixel stabilizes itself to a new dark current level. It can eventually disappear several days to years after its generation (Srouf et al. 2003). Most of this kind of evolution can be easily fitted and corrected by an exponential with a time constant of hours to weeks. The second curve shows that sometimes it is more complicated. We can see the bright pixel abruptly changing in intensity several times, probably due to successive rearrangements of the silicon defects. In the case of such noisy bright pixels, it is difficult to implement a correction.

A global characterization has been done with complete CCD images periodically acquired on sky in observation mode. Three sets of images (on exoplanet field, 32-s exposure time) with different dates are now available enabling some appreciation of the bright

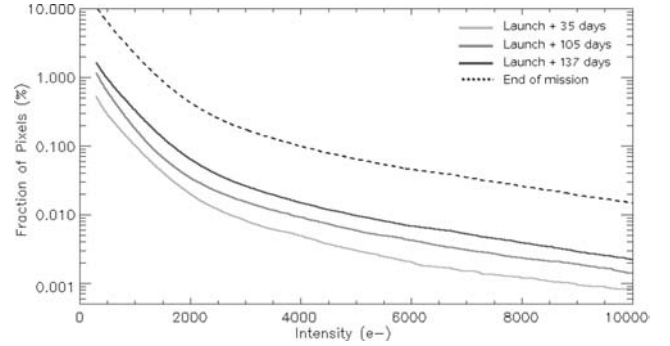


Figure 10. Statistical distribution of bright pixel intensities at three different dates (launch + 35 d, launch + 105 d and launch + 137 d). Dashed line is an extrapolation of the distribution at the end of the mission (launch + 2.5 yr)

Table 1. Bright pixels evolution and generation rate (above an intensity threshold).

	> 300 (e^- /exp)	> 1k (e^- /exp)	> 10k (e^- /exp)
Launch + 35 d	22314	320	6
Launch + 105 d	49026	1817	17
Launch + 137 d	69275	1817	17
Generation rate (per month)	15700	3100	21
End of mission (2.5 yr)	11 per cent	2.2 per cent	0.015 per cent

pixel evolution as a function of radiation dose. Isolated bright pixels have been extracted from full images and the distributions of their intensities are shown in Fig. 10. The three solid lines show the fraction of pixels on both exoplanet CCDs greater than a certain level on three different dates. They represent the tail integral of the dark current density which is proportional to the fluence (Hopkinson, Dale & Marshall 1996). Some quantitative figures are also given in Table 1. A preliminary extrapolation of the available data already suggests that bright pixels may represent a significant contribution to the photometric noise levels at the end of the mission (dashed line on Fig. 10), eventually representing an upper limit of the lifetime to the CCD detectors in space, given the current performance specifications. However, the strategy of annealing the CCDs remains possible, and could be employed if permanent radiation effects start to impose significant constraints on the accomplishment of the mission objectives.

5 CONCLUSIONS

We presented in this work an analysis of radiation effects on *CoRoT* images, in sight of the results obtained during the satellite's commissioning phase. The goal has been to present empirical data obtained in-flight, along with a discussion of the impact of these effects on precise and time-resolved stellar photometry from LEO. Additionally, we provided statistical information about the characteristics of particle impact trails on E2V-4280 CCDs, which might prove useful for future missions using similar technology.

In the case of *CoRoT*, we conclude that radiation can be a significant issue when very accurate photometry measurements are required, with precision specifications down to the shot noise level. The generation of spurious charge associated with a particle impact

leads to the systematic corruption of data whose significance will depend on the ability of identifying and correcting for it.

Finally, we have quantitatively described how permanent effects on the CCDs lead to a progressive loss of performance, an effect which can hardly be dealt with. Although some correction strategies can be implemented in the case of ‘well-behaved’ defects, some pixels present erratic behaviour after irradiation, and the Poisson noise associated with dark current is expected to steadily increase in any case. These facts illustrate how radiation effects can be critical in the design and exploitation of space-based instruments, in some cases significantly impacting their performances in the long term.

ACKNOWLEDGMENT

LPS was funded by the Brazilian Ministry of Science and Technology (CNPq grant No. 200334/2003-4). The authors would like to thank the whole *CoRoT* team for making possible the completion of this work.

REFERENCES

Boisnard L., Auvergne M., 2004, 55th Congress of the International Astronomical Federation (IAF), Corot Mission Engineering: Cost-Effective Solutions for Stellar Photometry in Low Earth Orbit. IAC-04-IAF-Q.1.01

E2V Technologies Ltd., 1998, CCD42-80 Back-Illuminated CCD Sensor Data Sheet, www.e2v.com
 Hopkinson G. R., Dale C. J., Marshall P. W., 1996, IEEE Trans. Nuclear Sci., 43, 614
 Jordan T. M., 2000, NOVICE: A Radiation Transport Shielding Code, Experimental and Mathematical Physics Consultants
 Letaw J. R., 1997, Space Radiation: A Commercial Code Available from Space Radiation Associates
 Olive D. J., 2005, Applied Robust Statistics, Applied Robust Statistics, preprint available online at <http://www.math.siu.edu/olive/>
 Srour J. R., Marshall C. J., Marshall P. W., 2003, IEEE Trans. Nuclear Science, 50, 653
 Wrobel F., 2005, Fundamentals on Radiation–Matter Interaction, New Challenges for Radiation Tolerance Assessment, RADECS 2005, Cap d’Agde, France

This paper has been typeset from a \TeX/L\AA\TeX file prepared by the author.